Toward Wide-Area Contactless Wireless Sensing

Lili Chen, *Member, IEEE, ACM*, Kai Chen, Jie Xiong, *Member, IEEE*, Ke Li, *Member, IEEE*, Sunghoon Ivan Lee, *Senior Member, IEEE, Member, ACM*, Fuwei Wang, Zhanyong Tang, *Member, IEEE, ACM*, Zheng Wang, *Member, IEEE, ACM*, Dingyi Fang, *Member, IEEE, ACM*, and Xiaojiang Chen, *Member, IEEE, ACM*

***Abstract*— Contactless wireless sensing without attaching a device to the target has achieved promising progress in recent years. However, one severe limitation is the small sensing range. This paper presents WIDESEE to realize wide-area sensing with only one transceiver pair. WIDESEE utilizes the LoRa signal to achieve a larger range of sensing and further incorporates drone's mobility to broaden the sensing area. WIDESEE presents solutions across software and hardware to overcome two aspects of challenges for wide-range contactless sensing: (i) the interference brought by device mobility and LoRa's high sensitivity; and (ii) the ambiguous target information such as location when employing just a single pair of transceivers for sensing. We have developed a working prototype of WIDESEE for human target detection and localization that are especially useful in emergency scenarios such as rescue search, and evaluated WIDESEE with both controlled experiments and the field study in a high-rise building. Extensive experiments demonstrate the great potential of WIDESEE for wide-area contactless sensing with a single LoRa transceiver pair hosted on a drone.**

***Index Terms*— Wide-area, wireless sensing, LoRa, mobility.**

I. INTRODUCTION

BESIDES traditional data communication functions, in recent years, wireless signals have been employed for sensing and have enabled diverse new applications including indoor navigation [24], [60], [65], health monitoring [9], [43], and human-computer interactions [16]. Wireless sensing relies on analyzing the characteristics of the signal reflected from the target to understand the contextual information of one's interest (e.g., localization). A wide range of wireless signals have been exploited for contactless sensing (i.e., without attaching any device to the target objects), including ultrasound and various types of radio frequency (RF) signals (e.g., WiFi and RFID). The RF signals attract particular attention in real-world sensing applications since they do not require to secure a Line-of-Sight (LoS) between the device and targets as opposed to conventional camera-based systems [41], and have stronger penetration capability compared to acoustic signals [49], [59].

Although promising, one evident issue with existing RF-based sensing is its limited sensing range, which hinders its applications in wide-area sensing such as disaster rescue. This is mainly because the signals reflected from the target, which contain information related to the context of the target, are much weaker than the direct-path signals between the transmitter and receiver. The fact that wireless sensing captures information from the reflected signals makes the sensing range much smaller compared to when the signals are used for communication purposes. For example, the current WiFi-based systems are only capable of performing sensing in a room-level range (i.e. approximately 3-6 m) [28], [60], whereas RFID or mmWave-based systems show an even smaller sensing range of 1-3 m [29], [54], [66].

Recently, efforts have been made to extend the contact sensing range of RF signals [12], [26], [67], [68]. Ashutosh *et al.* introduced an approach to employ multi-hop nodes to track the sensor-attached targets that are located deep inside a building structure [12]. In another example, Ma *et al.* leveraged drones to relay sensing information, which extends the sensing range from 5 m to 50 m [68]. Employing relay or multi-hop transmission schemes can increase the sensing coverage range. However, these approaches require deploying multiple devices as transceiver, which limits their applications in wide-area emergency rescue scenario for two reasons. On the one hand, multiple devices need to cooperate with each other, if the relay device or one inner node fails, the system will not able to achieve wide-area sensing; on the other hand, deploying multiple devices is time-consuming and therefore impractical in emergency rescue scenarios.

In this paper, we present WIDESEE, a contactless wireless sensing system, based on the emerging LoRa technology *with only a single transceiver pair*. WIDESEE is designed to push the boundary of wireless sensing. Our key insight is that the low-power, long-range wireless communication capability of LoRa offers a long propagation distance (i.e., several kilometers) and a strong penetration capability

Manuscript received 8 January 2021; revised 5 September 2021, 21 November 2021, and 24 March 2022; accepted 23 July 2022; approved by IEEE/ACM TRANSACTIONS ON NETWORKING Editor A. Khreishah. Date of publication 17 August 2022; date of current version 18 April 2023. This work was supported in part by the National Natural Science Foundation of China (NSFC) under Grant 62061146001 and Grant 61972316 and in part by the International Cooperation Projects of Shaanxi Province under Grant 2019KWZ-05 and Grant 2020KWZ-013. *(Lili Chen and Kai Chen are co-first authors.) (Corresponding author: Xiaojiang Chen.)*

Lili Chen, Kai Chen, Ke Li, Fuwei Wang, Zhanyong Tang, Dingyi Fang, and Xiaojiang Chen are with the School of Information Science and Technology, Northwest University, Xi'an 710069, China, and also with the International Joint Research Centre for Battery-Free IoT, Xi'an 710069, China (e-mail: llchen.nwu@gmail.com; ck@stumail.nwu.edu.cn; wfw@nwu.edu.cn; zytang@nwu.edu.cn; dyf@nwu.edu.cn; xjchen@nwu.edu.cn).

Jie Xiong and Sunghoon Ivan Lee are with the College of Information and Computer Sciences, University of Massachusetts Amherst, Amherst, MA 01003 USA (e-mail: jxiong@cs.umass.edu; silee@cs.umass.edu).

Zheng Wang is with the School of Computing, University of Leeds, Leeds LS2 9JT, U.K. (e-mail: z.wang5@leeds.ac.uk).

Digital Object Identifier 10.1109/TNET.2022.3196744

through obstacles, which in turn can be employed to significantly increase the sensing range compared to other wireless technologies. In this work, as a proof-of-concept, we explore the opportunities and limitations of the LoRa technology for non-contact human detection and localization in wide-area scenarios. To further increase the sensing area coverage, we leverage the mobility of a drone to carry the transceiver and move around the target area to perform wireless sensing. As we demonstrate later in this paper, we successfully realize building-scale, through-wall sensing to detect and localize human targets. We believe the proposed study is particularly useful for human target sensing (detection and localization) for applications in urban search and rescue missions.

Translating our high-level idea into a functional system, however, is nontrivial due to a number of challenges. First, the larger sensing range of LoRa also means the interference range is also larger due to the higher signal reception sensitivity. Second, a transceiver pair equipped with a single antenna does not provide us sufficient information regarding the target location since the number of unknown variables is greater than that of the constrained equations for localization. Third, although employing a drone can increase the sensing coverage, the vibration introduced by the drone during its operation (i.e., flying) affects the resultant signals and accordingly the target sensing performance.

To address the aforementioned challenges in wide-range sensing, we introduce solutions across the software and hardware stacks. To tackle the interference brought by LoRa's high sensitivity, we redesign the antenna system and the sensing algorithm. Specifically, we employ a compact, reconfigurable directional antenna at the receiver to narrow down the target sensing region. Our system can quickly (i.e., within $10\ ms$) switch the radiation pattern with a narrow beamwidth of $48°$. Such a design allows WIDESEE to stay focus on the area of interests and reduce the impact of interference. To further eliminate the multipath effect within the sensing area, we take a unique approach to first extract the direction-related information from available time-series of amplitudes and then use the information to isolate the target path from the interfering multipath. As a departure from the commonly used angle-of-arrival (AoA) or time-of-flight (ToF)-based methods, our design avoids the pitfall of relying on accurate channel phase information and large bandwidth, which are unfortunately not available on LoRa.

To reduce the ambiguities in localization, we build analytic models that can predict and determine target locations. This is based on our key observations that the speed of the moving target (e.g., humans) is relatively constant and the resulting trajectory is smooth within a short period of time (e.g., $< 1\ s$). We model the signal characteristics of the (vibration) noise and human target movements in frequency domain and filter out the vibration artifacts on the received signals to improve the sensing accuracy.

We integrate the proposed techniques to implement a working prototype and deploy it to detect and localize human targets in three different real-world environments: an open square, an underground parking garage, and a high-rise building structure with a size of $20 \times 42 \times 85\ m^3$. Our experiment results show that WIDESEE can effectively detect and localize human targets using just one transceiver pair. For 90% of the test cases, the localization error of WIDESEE is within $4.6\ m$. Such accuracy would allow one to identify at which room the human target locates in many typical building structures. This is a promising result considering we use only a single transceiver pair, and the target moves most of the time in a large environment. We hope this study can encourage further research in exploiting wide-area wireless sensing in detecting and tracking human targets to enable applications like disaster rescue search and security surveillance [55]. The main contributions of this paper can be summarized as followings:

- We present a contactless system for sensing human targets in a wide area using just one transceiver pair, by combining the agility of drone with the long-range propagation characteristic of LoRa.
- We introduce new algorithms and design methodologies across the software and hardware stacks to effectively tackle a series of interference issues when applying LoRa and a flying drone for wide-range sensing, and to address the sensing ambiguity issue when only one single transceiver pair is employed. The proposed techniques are generally applicable, and can be applied to other wireless sensing tasks.
- We demonstrate, for the first time, building-scale, contactless human sensing can be achieved with just one LoRa transceiver pair together with a drone. We can detect multiple targets simultaneously and localize one of them.

II. BACKGROUND AND OVERVIEW

A. LoRa Technology

LoRa offers a long communication range for up to several kilometers [51] with the ability to decode signals as weak as $-148\ dBm$. While the ability of decoding weak signals is beneficial for long range communications, it makes LoRa more likely to suffer interference from uninterested area in sensing. Even using a directional antenna at the receiver, there still exist strong multipath effects [31] within the detectable area that greatly affect the sensing accuracy. Much effort has been made to similar problems associated with multipath effects in other RF signals (e.g., WiFi [56] or RFID [69]) or acoustic signals [49], which are based on AoA or ToF information of the received signals. However, such information requires accurate channel phase readings and clock synchronization between the transmitter and receiver, both of which are unavailable on LoRa.

In this work, instead of making efforts on obtaining AoA or ToF to tackle the multipath effects, we consider an approach to leverage the received (albeit susceptible) signal strength (i.e., amplitude) for effectively addressing the inherent issue of multipath effects. This is described in Section III-C.

B. Motivation and Problem Scope

As depicted in the conceptual illustration in Figure 1, WIDESEE could be used to target emergency scenarios, such as disaster rescue and terrorist search in high-rise building structures. In these scenarios, identification of the presence of

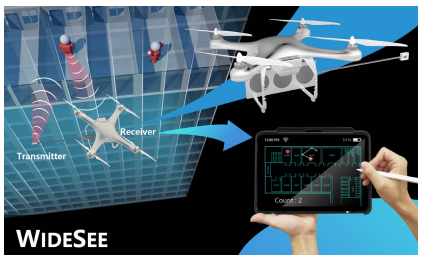

Fig. 1. Motivation example of WIDESEE: a building-scale human target sensing scenario.

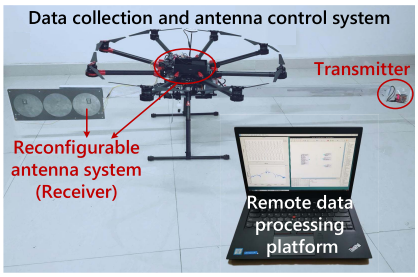

Fig. 2. Overview of WIDESEE. We use a drone to carry the LoRa transceiver pair and its control system. The data are sent back to the remote data processing platform to perform real-time target detection and localization.

human targets and their locations is of high importance, but doing so is challenging because (a) the localization sensing infrastructure (e.g., surveillance cameras) may not be readily available or has been destroyed, and (b) visual inspection of human targets is restricted if not impossible. WIDESEE is designed to offer decision supports in such difficult settings.

In our application of human sensing, we aim to achieve the following two goals. The first is to detect the existence of human targets. The second is to identify the target's location if a presence is detected. We do not consider a multiple-device or multi-hop transmission scheme, because such a strategy requires a careful and complex setup process, which is often infeasible in emergency situations. As a proof-of-concept, WIDESEE is designed to be capable of detecting the presence of multiple human targets located in different rooms in the same building, but only localizing one target at a time. We leave the simultaneous localization of multiple targets as our future work.

C. Overview of WIDESEE

WIDESEE is a wide-range contactless human target sensing system built upon a single LoRa transceiver pair. The transceiver pair (both the transmitter and receiver) is carried by a drone so that WIDESEE can scan and sense a large area by flying the drone. Having a small, lightweight design for WIDESEE is essential to maintain a good endurance for the battery-powered drone.

WIDESEE operates by first transmitting the LoRa signal, and then capturing and analyzing the received resultant signal from the direct signal path and reflections off the target and surrounding objects. To detect the presence of a human target, WIDESEE models how a human activity like breathing, waving or ambulating affects the power spectral density (PSD) of the received signal. WIDESEE then tries to locate a detected human target by extracting and analyzing the target's direction-related information. As depicted in Figure 2, WIDESEE consists of three innovative components:

- A *compact, reconfigurable antenna system* to reduce the interference from uninterested areas. To prevent moving targets from being missed, the antenna should be able to adjust its direction and radiation pattern quickly. Our design is detailed at Section III-A.
- A *data collection and antenna control system*, which includes a LoRa transceiver pair, a data collection subsystem, and a drone. The drone carries the LoRa transceiver pair and the data collection subsystems to fly around the target region. The collected LoRa signal data are sent back to a laptop (through a LTE network) to be processed on the ground. The antenna control system employs an Arduino board carried by the drone to configure the antenna radiation pattern accordingly. The details are described in Section III-B.
- A *target detection and localization system*, which runs on a data processing platform, i.e., a laptop in our case. The system analyzes the collected data to detect and localize the human target. This is discussed in detail in Section III-C.

III. SYSTEM DESIGN OF WIDESEE

WIDESEE leverages LoRa's long communication range and high penetration capability for sensing targets that are within a wide area or deep inside building structures. As discussed in Section II-A, this advantage also brings in more interference from uninterested objects due to the larger sensing range. Overcoming this limitation requires novel design methodologies, analysis and processing algorithms.

A. Reconfigurable Antenna System

To reduce the interference, we look for innovations at the antenna side. Our first intuition is to employ a directional antenna at the receiver to narrow down the sensing region. However, commonly used horn directional antennas such as RFMAX [5] have a fixed radiation pattern and mechanically rotating the antenna orientation to focus on a region is too slow. Furthermore, the beamwidth offered by a horn antenna is usually not narrow enough [5]. An alternative is to use a phased-array antenna that can change the radiation pattern by adjusting the amplitude and phase of each antenna element, to achieve fast scanning with narrower beams [21], [27]. However, there is a problem for using a phased-array antenna with LoRa. The LoRa signal has a wavelength of 33 cm and to achieve a 25° beamwidth, the linear array will have a size of approximately 2 m. The resulted antenna design is not only expensive, but also too bulky to be fitted on a domestic drone.

We wonder if we could bring together the advantages of horn antenna (small size and low cost) and phased array (high resolution and scanning speed). In answer, we adopt a reconfigurable antenna approach [14], which is capable of switching

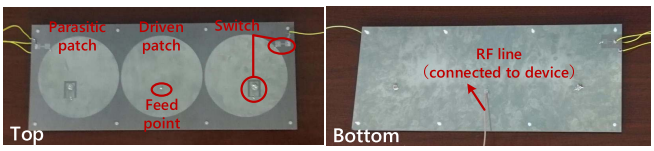

Fig. 3. The fabricated antenna system on the receiver side.

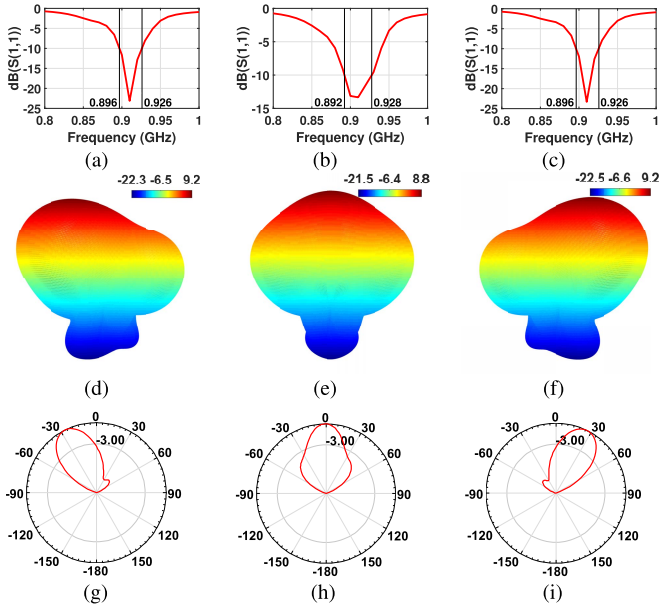

Fig. 4. Frequency and radiation properties of our reconfigurable antenna system. Here (a–c), (d–f) and (g–i) respectively represent the frequency property, radiation pattern and normalized radiation pattern of mode1-3.

the radiation pattern and frequency properties through adjusting its internal current flow distribution to offer a narrow beamwidth.

Specifically, we choose to use a parasitic-planar-patch antenna [30] for our reconfigurable antenna design. Figure 3 shows our reconfigurable antenna implementation that is used at the receiver side, which consists of a driven patch in the center and two parasitic patches on both sides. Beam steering is achieved by manipulating the status of the parasitic patches to act either as reflectors (when shorted to ground) or directors (when not shorted to ground). The radius of each patch is 78 mm. Two shorting pins are shorted to ground from each parasitic patch, to ensure that the currents can flow from the parasitic patches to the ground according to the RF switching configuration. Two SMP1345 PIN diode switches are soldered on the parasitic patch layer close to each of the shorting pins and the RF/direct-current (DC) input. Each diode occupies a small space of around 2×2 mm. The PIN diode is achieved by using a resistance (1.5 Ω) and a capacitor (1.5 pF) for ON and OFF states, respectively. The resulting antenna system is small (20×50 cm) and has a comparable weight to a similar-sized horn directional antenna (< 1 kg), but has the advantage of quickly switching the radiation patterns. It costs us less than 300 USD to build the antenna and its control system, and we expect the price to be significantly reduced during massive production.

TABLE I

PROPERTIES OF OUR ANTENNA SYSTEM AND A SIMILAR-SIZED RFMAX [5]—A POPULAR HORN DIRECTIONAL ANTENNA

	Frequency range (MHz)	Gain (dBic)	Beamwidth (at 3 dB)	Size (cm^3)
WIDESEE (mode 1)	896-926	9.2	48°	
WIDESEE (mode 2)	892-928	8.8	45°	$20 \times 50 \times 1$
WIDESEE (mode 3)	896-926	9.2	48°	
RFMAX	902-928	9	70°	$26 \times 26 \times 5$

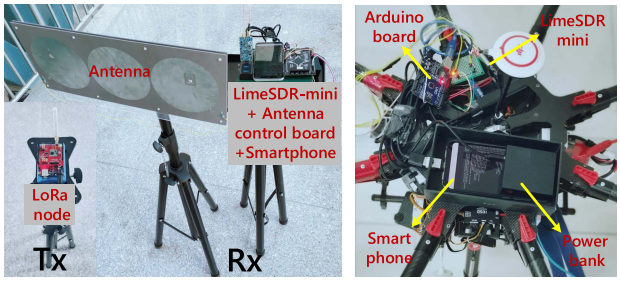

(a) The transceiver pair (b) Data collection and control

Fig. 5. We use a DJI S1000 to carry the LoRa transceiver pair (a) and the data collection/control subsystem (b).

Figure 4 shows the frequency and radiation properties of our antenna system. Our current implementation supports three different radiation modes. We use an Arduino board to switch between the three modes in a round-robin fashion, where switching occurs every 10 ms. We empirically determined this switching frequency which is sufficient for sensing human targets. This is based on the observation that the human body movements often have a frequency less than 10 Hz [19].

Table I compares our antenna system (in three different modes) against a similar-sized RFMAX [5] – a widely used horn directional antenna. From the table, we see that the frequency range and gain of our antenna system for the three modes are comparable to those of RFMAX, but our design has the advantages of offering quick radiation pattern switching and a narrower beamwidth. These advantages make our antenna system more suitable for target sensing with LoRa. Note that, the total radiation angle range of our system is twice RFMAX's, and the radiation pattern switching is much quicker (i.e., 10 ms) than horn antenna which requires mechanical rotation for direction change.

B. Data Collection and Antenna Control System

As depicted in Figure 2, we use a consumer drone to carry the transceiver pair and its control and data collection modules.

1) Transceiver Pair: Our LoRa transceiver pair is shown in Figure 5 (a). We use an off-the-shelf device, Semtech SX1276 [6], with an omnidirectional antenna as the LoRa signal transmitter. The transmitter sends signals in a continuous mode at 890 MHz frequency – the best working frequency of our reconfigurable antenna system. At the receiver end, we use LimeSDR-mini (a software-defined radio board [4]) as the LoRa gateway to collect signal at a sampling rate of 250 KHz through running the GNU radio software development toolkit [2]. We connect the board to our reconfigurable

antenna (see Section III-A) through one of its RF connectors, and to an Android smartphone (with $8G$ of RAM and $128G$ of storage) via a USB 3.0 port.

The receiver end works as follows. After initializing the LimeSDR-mini board, the antenna control software running on the Arduino board continuously switches among the three radiation modes of the antenna, at a frequency of 10 ms. The detection area was roughly divided into three-part and each part matches a radiation pattern of the reconfigurable antenna. When the host computer changes the radiation pattern, the system will clear the sampling buffer and re-sample the signal in the current radiation pattern. The collected samples are read by the smartphone to be transferred (labeled with the radiation modes) to a laptop via LTE connection for data processing. In this way, WIDESEE can detect and localize targets within an interested area covered by each radiation mode. Note that it is possible for our target detection and localization algorithms to run on the smartphone or an embedded device to remove the need of data transfer, and we leave this as our future work.

2) Drone System: We use a DJI S1000 drone [7] to increase the area a single transceiver pair can effectively cover. As illustrated in Figure 5 (b), the LimeSDR-mini, smartphone, Arduino board are put on top of the drone and are powered by a $5200\ mAh$ portable power bank with a $2.4\ A$ output. We employ the collision avoidance system provided by DIJ to avoid drone collision with obstacles. The drone is controlled by software running on a laptop, programmed through the DJI software development kits. One limitation of the drone system is that it can not operate for a long time when loaded with the devices and one battery charge can support around 15 minutes of flight. Our future implementation will look into reducing the drone's load by running the data collection and antenna control software on a single computing device (e.g., the Arduino board), which can be powered directly by the drone's battery. Multiple drones can be utilized to alleviate this power-hungry issue.

C. Target Detection and Localization System

We develop a set of algorithms to process the collected LoRa signal data to detect and localize human targets. The process of detection and localization works as follows. We first pre-process the received signal to remove the noises caused by the drone's vibration artifacts. We then exploit the power spectrum density (PSD) of the processed signal to detect the presence of human targets. The PSD is calculated as the Fast Fourier Transform (FFT) of signal amplitudes' self-correlation. Note that our detection mechanism can detect the presence of target no matter one or multiple targets are present in the sensing area. After detecting the presence of a moving target, we apply the localization algorithm to estimate the location of the target whose reflection is strongest at that time. Note that during the localization stage, we let the drone hover in place. With the device mobility, we can detect and locate multiple targets successively. As we have previously discussed, WIDESEE needs to effectively handle the multipath effects and location ambiguities brought in by using only one LoRa transceiver pair.

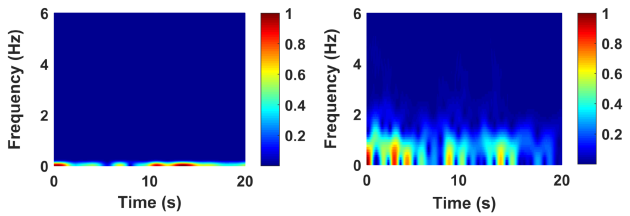

(a) Without human target. (b) With a moving human target.

Fig. 6. Comparison of the PSD of the received signal when there exists no human target (a) and a moving target (b). The PSD patterns in two scenarios differ significantly. WIDESEE exploits this observation to detect the presence of human targets.

1) Vibration Noise Elimination: Vibrations of a flying drone inevitably introduce noise to the received LoRa signals. To remove the introduced noise, we exploit the observation that the motion artifacts brought by a drone are within a frequency range between $60\ Hz$ and $150\ Hz$, which is different from the lower frequency range of a human body movement ($< 10\ Hz$). Therefore, we first use a low-pass filter (i.e., second-order Butterworth low pass filter with a cutoff frequency of $10\ Hz$) to remove the high-frequency motion artifacts in the frequency domain and then convert the filtered signal back to the time domain to be processed in the next stage. Our evaluation in Section IV shows that this is a simple yet effective strategy.

2) Human Target Detection: Human activities like hand waving and walking will alter the wireless propagation paths and lead to the change of signal amplitude at the receiver [11]. Prior work shows that when no human target is present, the received signal can be approximated as the superposition of constant signals and the white Gaussian noise, yielding an invariant PSD with time [45]. By contrast, the PSD of the received signal resulted from a moving human target, will lead to fluctuations on the measured signal. As an example, consider Figure 6 drawn from our own experiments. It illustrates the difference in the PSD with and without a moving human target. When no human target is present (Figure 6 (a)), the PSD of the received signal remains stable with time and close to $0\ Hz$, while when a moving target presents (Figure 6 (b)), the PSD fluctuates at low frequencies ($0 - 10\ Hz$). Our work exploits this signal characteristic to detect the presence of a human target – if the measured PSD frequency and its variance are both below a threshold (empirically set to $0.1\ Hz$ in our case), we consider there is no human target; otherwise, we conclude that someone (with movements) is in the sensing area.

In this work, we focus on detecting human targets with large movements: ambulating or waving in-place. We are also able to detect a stationary breathing target when there is no obstacle between the transceiver pair and the target, or the obstacle is thin (see Section IV-B.3). Figure 7 illustrates the normalized PSD of the reflected signals of these three states (ambulating, waving and stationary) from a human target in a controlled environment. The diagram shows that different states exhibit different characteristics in the frequency domain, which can be used to identify and differentiate these states. In particular,

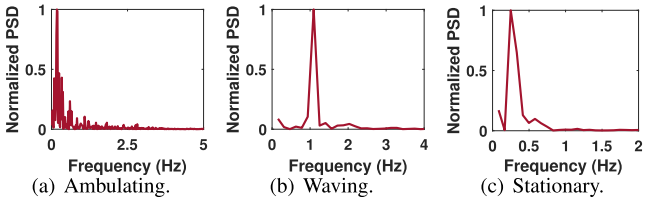

Fig. 7. Frequency distribution of signal changes caused by three states of a human target. Different states lead to different signal frequency distributions.

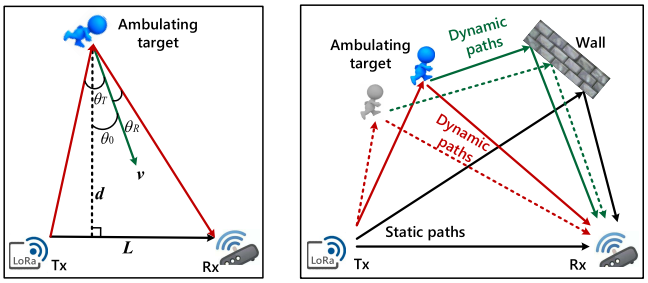

Fig. 8. (a) shows the setup of moving target localization. Similar to the linear virtual array constructed by moving receiver. The moving target also can emulate a linear array. (b) presents the superposition signal of multiple paths.

human breath and waving present strong, dense PSD with a frequency range of 0.1-0.6 Hz and 1-4 Hz, respectively. By contrast, the PSD distribution of an ambulating human target is more spread apart, mainly due to the human target's randomized ambulatory trajectory pattern and uncorrelated movements of multiple body parts.

Multi-target identification. In Section 3.3.2, we showed how to detect the human target presence. Then a natural question is: how many targets are there inside the sensing area? Since only one antenna is used for both transmitter and receiver, the observation angle is limited, the reflected signals from multiple targets may not all reach the receiver. Also there exits mutual interference between different targets. These factors make it difficult for us to identify the number of targets according to the number of PSD peaks. Fortunately, the human target motion is continuous across a short period of time, thus we propose to combine the time domain amplitude change and frequency domain PSD pattern during multiple time segments to identify the number of human targets. We input both the time and frequency domain features to the support vector machine (SVM) to obtain the number of targets.

3) Ambulating Target Localization: Once the ambulating human target is detected, we focus on identifying the location of the target. One of the technical challenges in LoRa-based target localization is that the multipath in LoRa is more severe than that in other signals (e.g., WiFi). Even though we utilize the narrower beam antenna at the receiver, the multipath within the sensing area can be still substantially strong, which negatively impacts target localization. To address the multipath issue for localization, previous work has investigated various techniques, such as analyzing the AoA information [61], frequency hopping based on accurate channel phase measurement [39], [44], and comparing ToF that requires large bandwidth and tight transceiver synchronization [34]. Unfortunately, these techniques are not applicable to our system because the maximum bandwidth of LoRa is only 500 KHz, and the asynchronism between LoRa node (Tx) and gateway (Rx) makes it difficult to extract stable phase readings from the received signal. Also, it is particularly difficult to achieve synchronization between LoRa node and gateway due to the cheap oscillator adopted. Because of the chirp modulation scheme adopted, LoRa can tolerate high frequency offset for communication so high-accuracy oscillator is not needed.

In this work, we propose an amplitude-based anti-multipath method to localize a moving target. The foundation of our method is to extract direction-related information from signal amplitudes, inspired by the recent work [32], [46]. By using the direction-related information for localization, we have the opportunity to remove the multipath effect that however is not addressed well in [32] and [46]. In the following subsections, we first describe the basic concepts behind extracting the direction-related information when a target is moving. Then, we answer how to obtain target location information from the extracted direction-related information. Finally, we propose the solution to handle multipath.

Direction-related parameter estimation. Here we first describe the framework for estimating direction-related parameter in device moving scenario (target does not move), which can be used to deduce the direction-related parameter in target moving case (device does not move).

Considering a scenario in which we have one receiver that receives signals from K different sources. When the receiver moves along a straight line at a speed v, it can emulate a linear array. We can define the incoming angle of each signal source in far-field as θ_k, $k = 1, 2, \ldots, K$. Then, the signal received from the k^{th} source at time t can be expressed as $x_{t,k} = a_{t,k}e^{j(\mu_k + \frac{2\pi vt}{\lambda}cos\theta_k)}$ [23], where $a_{t,k}$ is the amplitude of the signal and μ_k is the signal phase at the initial time point (i.e., $t = 0$). Then, the signal received at the receiver at time t is a superposition of K signals, which can be written as:

$$y(t) = \sum_{k=1}^{K} a_{t,k}e^{j(\mu_k + \frac{2\pi vt}{\lambda}cos\theta_k)}. \tag{1}$$

Let us denote $R(\tau)$ as the self-correlation of the received signal amplitudes at delay τ. Then, $R(\tau)$ can be expressed as [23], [32]:

$$R(\tau) = C_A + \sum_{k=1}^{K-1}\sum_{j=k+1}^{K} C_{k,j} \cdot cos\left(2\pi\frac{v\tau}{\lambda}(cos\theta_k - cos\theta_j)\right), \tag{2}$$

where C_A is a constant term depending on the total signal power and $C_{k,j} = \frac{\pi a_{t,k}^2 a_{t,j}^2}{16\sum_{k=1}^{K} a_{t,k}^2}$, where $a_{t,k}^2$ is the signal power of k^{th} signal. It is noteworthy that $R(\tau)$ consists of a total of $\frac{K(K-1)}{2}$ harmonics. Each harmonic's frequency is related

to the cosine of two sources' AoAs (i.e., θ_k, θ_j, and $k = 1, 2, \ldots, K$, $j = 1, 2, \ldots, K$), which is given by:

$$\widetilde{f_{k,j}} = \frac{v}{\lambda}|cos\theta_k - cos\theta_j|. \tag{3}$$

Note that $cos\theta_k$ and $cos\theta_j$ are unknowns we are trying to obtain the values. These frequencies $\widetilde{f}_{k,j}$ can be obtained by the frequency estimation technique, such as the fast Fourier transformation of amplitudes' self-correlation followed by a peak magnitude detection.

For the target moving and transceiver fixed scenario shown in Figure 8 (a), the resultant signal is composed of reflection (Tx $\rightarrow$ target $\rightarrow$ Rx) from an ambulating human target and direct path (Tx $\rightarrow$ Rx). The resultant signal at time t can thus be written as:

$$y(t) = a_s e^{j\mu_s} + a_d e^{j\left(\mu_d + \frac{2\pi vt}{\lambda}(cos\theta_T + cos\theta_R)\right)}, \tag{4}$$

where a_s and μ_s are the amplitude and phase of the direct path signal, a_d is the amplitude of the signal reflected from the moving target, μ_d is the initial phase ($t = 0$) of the reflected signal, v is the moving speed of the target, θ_T and θ_R are two angles marked in Figure 8 (a).

Equation (4) is a special case of Equation (1) with 2 sources ($K = 2$), $cos\theta_1 = 0$ and $cos\theta_2 = cos\theta_T + cos\theta_R$. The moving target can synthesize a transmitter array. We put $cos\theta_1$ and $cos\theta_2$ into Equation (3) to obtain the following:

$$\widetilde{f_{1,2}} = \frac{v}{\lambda}|0 - (cos\theta_T + cos\theta_R)|, \tag{5}$$

since v, θ_T and θ_R are unknowns in practice, we jointly estimate the direction-related parameter $|v(cos\theta_T + cos\theta_R)|$ as $\widetilde{f_{1,2}}\lambda$ according to Equation (5).

Localization ambiguity avoidance. By utilizing the $|v(cos\theta_T + cos\theta_R)|$ estimate from only one transceiver pair to localize the target, there exist severe localization ambiguities that stem from three aspects: (1) the absolute value symbol $|\ |$ applied to $v(cos\theta_T + cos\theta_R)$; (2) unknown distance d between the target and the Tx-Rx LoS link as shown in Figure 8 (a); and (3) unknown speed v and direction θ_0 of target movement. We show the localization result of a special case ($\theta_0 = 0$) in Figure 11 (a). We can see that even with $\theta_0 = 0$ to simplify the problem, there still exist ambiguities (the areas with red color). So it is difficult to obtain the target's true initial location.

In this paper, we solve this problem based on the facts that the target's moving trajectory is smooth and the velocity is a constant during a short period of time (e.g., < 1 s). Specifically, we utilize multiple consecutive estimates of $v(cos\theta_T + cos\theta_R)$ with a sliding window of size w, and each estimation process requires samples collected in a time window of size τ. w and τ are empirically set as 0.25 s and 1 s in our system. To reduce the computational time, we reduce the sample rate from 250 KHz to 1 KHz for PSD calculation. For a desired frequency resolution, we set the number of transformation point as 2^{15} in FFT procedure. We aim to solve five unknown parameters: $[\theta_{T1}, \theta_{R1}, \theta_0, d_1, v]$, where θ_{T1}, θ_{R1} and d_1 are the initial values of θ_T, θ_R and d respectively. Note that within a short period of time, v and θ_0 can both be considered as constants while θ_T, θ_R and d are changing. During the process

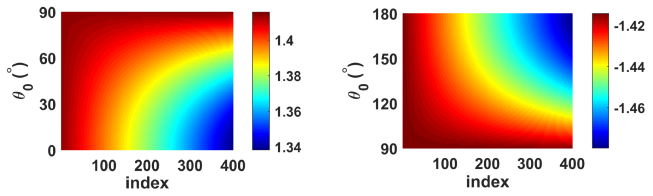

(a) Target moves towards LoS. (b) Target moves away from LoS.

Fig. 9. The changing trend of $v(cos\theta_T + cos\theta_R)$ estimates at various target moving directions θ_0. It can be seen that the changing trend of $v(cos\theta_T + cos\theta_R)$ estimates from the 1st to m^{th} is always *decreasing* no matter the target moves towards LoS ($0° < \theta_0 < 90°$) or moves away from LoS ($90° < \theta_0 < 180°$).

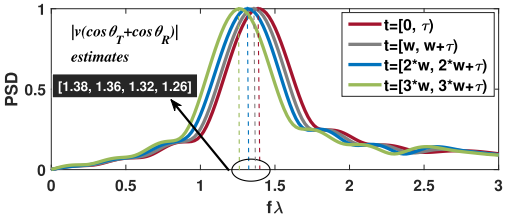

Fig. 10. Four adjacent estimates of direction-related parameter $|v(cos\theta_T + cos\theta_R)|$. The estimates are the normalized frequencies corresponding to the peaks of PSD plots.

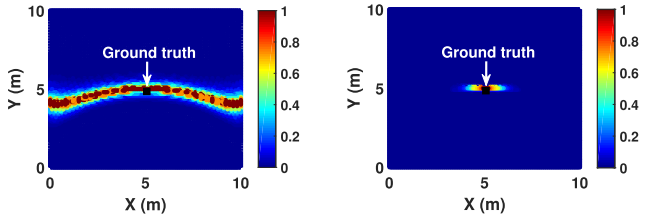

(a) Before ambiguity avoidance. (b) After ambiguity avoidance.

Fig. 11. Localization ambiguity avoidance. The heatmap exhibiting the likelihood that how a partitioned grid is likely to be the initial location of the target. The coordinates of Tx and Rx are $(0, 0)$ and $(10, 0)$, the ground truth is highlighted with black square. From (a), we can see all grids of the reddest color result in the same value of $|v(cos\theta_T + cos\theta_R)|$, resulting severe localization ambiguities.

of target movement within a short period of time, we keep estimating the three changing variables. For the m^{th} estimate, we can have the two equations bellow:

$$\begin{cases} v(cos\theta_{Tm} + cos\theta_{Rm}) = \pm(\widetilde{f_{1,2}}\lambda)_m \\ d_m(tan(\theta_0 + \theta_{Rm}) + tan(\theta_{Tm} - \theta_0)) = L. \end{cases} \tag{6}$$

Note that $\pm$ can be removed due to our observation as shown in Figure 9. We find that the changing trend of $v(cos\theta_T + cos\theta_R)$ estimates from the 1st to m^{th} are always *decreasing*. When the target moves towards transceiver pair, the values of $\cos\theta_T$ and $\cos\theta_R$ ($0° < \theta_T < 90°$, $0° < \theta_R < 90°$) are positive and the values decrease with angles θ_T and θ_R increasing. When the target moves away from the transceiver pair, the values of $\cos\theta_T$ and $\cos\theta_R$ ($90° < \theta_T < 180°$, $90° < \theta_R < 180°$) are negative and the values again decrease with angles increasing. So we delete another set of estimates that do not satisfy the condition of *decreasing* from the 1st to m^{th} estimates.

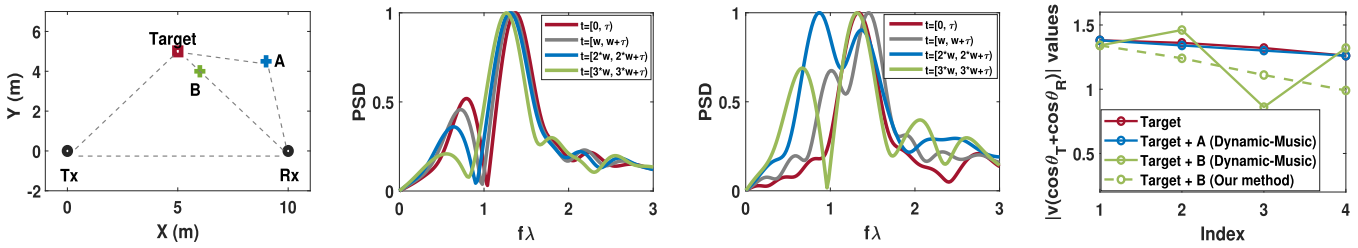

(a) Setup. (b) PSD plots with interfering object at location A. (c) PSD plots with interfering object at location B. (d) $|(v(cos\theta_T+cos\theta_R))|$ estimates.

Fig. 12. Multipath interference presentation. The figure shows that past AoA based multipath removal solution fails when the interfering object is close to the connecting line between target and receiver/transmitter (like at location B). Our approach has the ability to mitigate the problem.

Consider the fact of trajectory smoothness and speed constancy over a short period of time, we can add the following constraints:

$$\begin{cases} \theta_{Tm} \approx \theta_{T1} + (m-1)\alpha \\ \theta_{Rm} \approx \theta_{R1} + (m-1)\beta \\ d_m \approx d_1 - v\tau(m-1)cos\theta_0, \end{cases} \tag{7}$$

where α and β are constant but unknown. By incorporating Formula 7 into Formula 6, we find that when m reaches 4, the number of equations ($2m = 8$) is larger than the number of unknowns (a total of 7 with 5 original unknowns and 2 newly introduced unknowns). Thus we are able to solve the unknowns with only 4 estimates of $|v(cos\theta_T + cos\theta_R)|$ as shown in Figure 10.

Since the equations are non-linear that cannot be solved directly, an intuitive choice is to use Approximate Search algorithm. To avoid the local optimum issue and reduce time overhead, we adopt Particle Swarm and Global Search from Matlab Global Optimization Toolbox to achieve global optimum search for the set of non-linear equations. The principle is to obtain an initial search value close to the solution using particle swarm, then limit the objective function with fmincon's non-linear constraints, and finally use Global Search to obtain the solution. The computational complexity of the search algorithm is $O(N \times M)$, where N is the dimension of the particle swarm and M is the number of iterations. Specifically, we set the number of particles N and the number iterations M as 70 and 1400, respectively. And we allow the inertia coefficient change from 0.1 to 1.1. The inertia coefficient will be updated smoothly at each iteration with a dynamic factor. In addition, we set a boundary for each searching variable according to the actual condition, which reduces the scale of the searching problem. Figure 11 (b) shows that the initial localization result with our ambiguity avoidance scheme is close to the ground-truth.

Multipath interference elimination. Consider a typical multipath scenario shown in Figure 8 (b), we can see that the received signal at the receiver is a superposition of multiple signals, which can be written as:

$$y(t) = a_s e^{j\mu_s} + a_d e^{j(\mu_d + \frac{2\pi vt}{\lambda}(cos\theta_T + cos\theta_R)} + a'_d e^{j(\mu'_d + \frac{2\pi vt}{\lambda}(cos\theta'_T + cos\theta'_R)}, \tag{8}$$

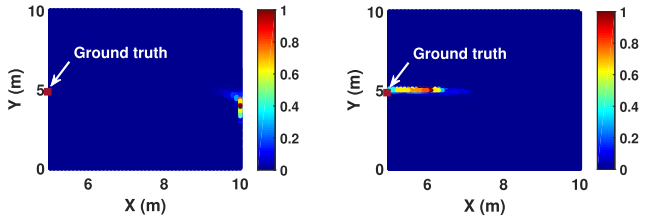

(a) Using Dynamic-Music. (b) Using our approach.

Fig. 13. Localization errors of using past (5.1 m) and our (1 m) multipath elimination approaches, when an interfering object locates at point B as shown in Figure 12 (a).

where a_d, μ_d, θ_T and θ_R are the amplitude, initial phase ($t = 0$), angle parameters of the direct target reflection (Tx→target→Rx), respectively. To simplify representation, here we approximate the indirect target reflection (Tx→target→wall→Rx) as a new direct reflection from a virtual target (Tx→virtual target→Rx), with amplitude a'_d, initial phase ($t = 0$) μ'_d, direction parameters θ'_T and θ'_R. In such scenario, the $\widetilde{f}\lambda$ value set has $|v(cos\theta_T + cos\theta_R)|$ as well as $|v(cos\theta'_T + cos\theta'_R)|$ and $|v(cos\theta_T + cos\theta_R) - v(cos\theta'_T + cos\theta'_R)|$ components. Since the resultant static component (contains direct path) is much stronger than the reflections, we can lock the two dominant $\widetilde{f}\lambda$ estimates as $|v(cos\theta_T + cos\theta_R)|$ and $|v(cos\theta'_T + cos\theta'_R)|$.

To distinguish the target corresponding $|v(cos\theta_T + cos\theta_R)|$ value from the $|v(cos\theta'_T + cos\theta'_R)|$ estimate shown in Figure 12 (b-c), existing solutions (e.g., Dynamic-Music) exploit the fact that the direct target reflected path is stronger than the indirect target reflected path [38], [53], [61] due to the shorter path of former, so they consider the $\widetilde{f}\lambda$ value of larger magnitude as the direct target reflection resulted $|v(cos\theta_T + cos\theta_R)|$.

This approach can be effective when the interfering object (at location A in Figure 12 (a)) is far away from the connecting line between target and receiver/transmitter. We can see that the four estimates of $|v(cos\theta_T + cos\theta_R)|$ decrease monotonically as shown in Figure 12 (d) when there is one interfering object at location A. Figure 12 (b) shows the PSD plots and the position ($\widetilde{f}\lambda$) of the peak is the estimate. We can see that for 4 consecutive time window, the ($\widetilde{f}\lambda$) is decreasing. These results are similar to the case when there is no interfering object. However, when the interfering

object (at location B in Figure 12 (a)) is close to the connecting line between target and receiver/transmitter, the $|v(cos\theta_T + cos\theta_R)|$ estimates show remarkable shifts as shown in Figure 12 (c) and (d) and thus fail to localize the target. To mitigate this problem, instead of taking the peak value position $\widetilde{f}\lambda$ shown in Figure 12 (c) as $|v(cos\theta_T + cos\theta_R)|$, we take the average of two positions corresponding to largest and second largest peak values as $|v(cos\theta_T + cos\theta_R)|$ if we find the four estimates are not decreasing monotonously and the second largest peak value is larger than 50% of the largest peak value. The reason for this is that when the interfering object is at location B, the length of the target dynamic path is similar to that of the interfering dynamic path. In this case, using a median frequency value can correct the frequency bias caused by the interference between two frequencies that are too close to each other. Figure 12 (d) shows that by using our methods to obtain the new $|v(cos\theta_T + cos\theta_R)|$, the 4 estimates now decrease monotonously and match the no-interfere estimates much better than those obtained with the Dynamic-Music method. The localization error of our method ($1\ m$) is much lower than that of Dynamic-Music method ($5.1\ m$).

IV. Evaluation

A. Experiment Setup and Roadmap

We performed two sets of field experiments to evaluate WideSee in detecting and localizing human targets: field experiments without a drone and field experiments with a drone.

1) Field Experiments Without a Drone: We would like to provide a quantitative evaluation first to justify our design choices, and to identify the research opportunities and limitations of LoRa sensing. To this end, we evaluate how the distance between transmitter and receiver affects the sensing range of LoRa in Section IV-B.1. In Section IV-B.2, we report the performance of our antenna design for detecting moving human targets and compare it with two alternative designs using omni- and horn-directional antennas. We then evaluate LoRa's penetration capability in detecting three different human activities in Section IV-B.3, before reporting the localization accuracy of our system in Section IV-B.5. Finally, in Section IV-B.6, we evaluate the impact of the human target's walking speed on detection and localization accuracy. Controlled experiments were performed on the ground for detecting a single moving human target with the LoRa transceiver pair placed $1\ m$ above the ground.

2) File Study With a Drone: In the field study, we use a drone to carry the LoRa transceiver pair to detect and locate a human target in the building shown in Figure 14 (c). We report the performance for detecting the presence of human targets and the accuracy for localizing a human target with different drone speeds. The results are given in Section IV-C.

3) Evaluation Metric: We calculate the accuracy for detecting the presence of a human target as:

$$Accuracy = \frac{1}{C}\sum_{c=1}^{C}(1 - |\frac{H_{m,c} - H_{t,c}}{H_{t,c}}|), H_{m,c}, H_{t,c} = \{0, 1\}$$

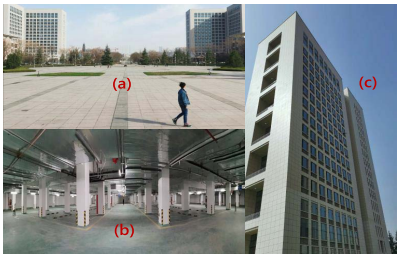

Fig. 14. Evaluation scenarios. We evaluate WideSee in an open square (a), an underground parking garage (b), and a middle floor of a 17-floor building (c). The testing area is on one side of the transmitter-receiver line in all of the experiments.

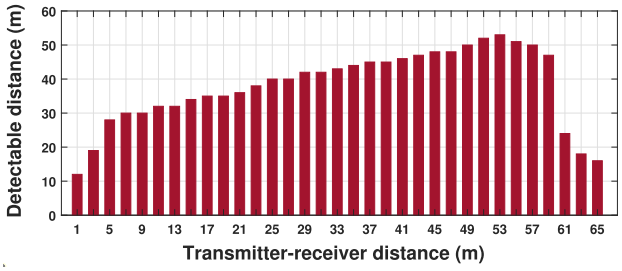

Fig. 15. Impact of the transmitter-receiver distance on the detectable distance (sensing range). WideSee can detect a moving object with a distance to the transceiver pair of up to $53\ m$ in an open square.

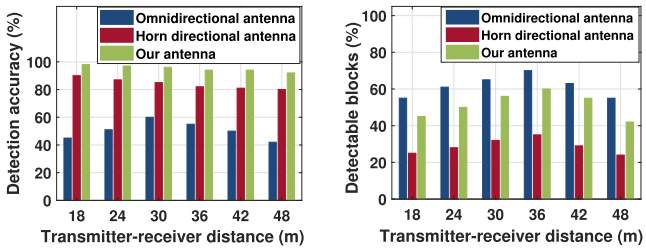

(a) Detection accuracy. (b) Detectable area.

Fig. 16. Comparing the detection accuracy (a) and region (b) between our approach and alternative directional antennas with a similar size. Our antenna design gives the best trade-off between the detection accuracy and range.

where C is the number of tests, $H_{m,c}$ and $H_{t,c}$ are the outputs of WideSee and the ground-truth in the cth test respectively.

B. Field Experiments Without a Drone

1) Sensing Range Under Different Transmitter-Receiver Distances: In this experiment, we varied the transmitter-receiver distance, i.e., the distance between the transmitter and the receiver, from $1\ m$ to $65\ m$ at a step size of $2\ m$. The tests were conducted in the open square shown in Figure 14 (a). In each transceiver pair setting, we asked a target to walk along the vertical bisector of the transceiver pair 100 times with a walking distance of $3\ m$ each time, starting from a randomly chosen position. Note that we moved the starting point further from the transceiver pair each time, until we fail to detect the user at that point. We consider a position to be detectable if we can correctly detect the user at that position for over 90% of the time. We calculated the distance between each detectable position and the middle point of the transceiver pair link to

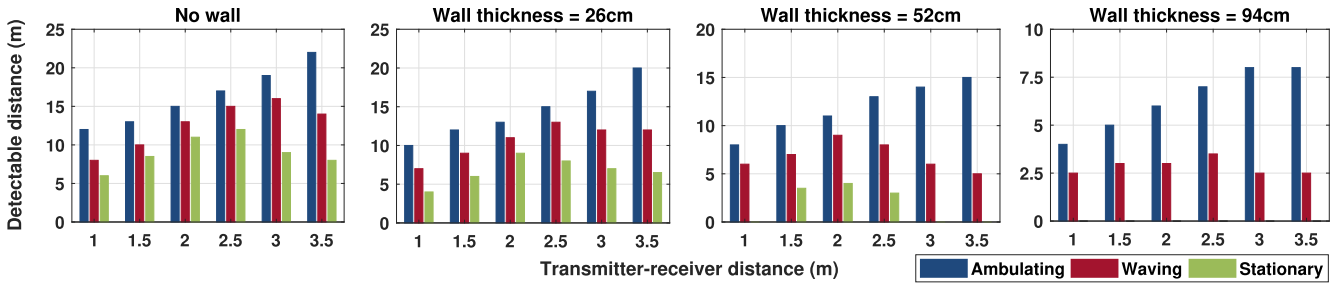

Fig. 17. Penetration test. WIDESEE can detect a stationary human target who is behind a wall with a thickness of 52cm, and WIDESEE can detect a moving/walking target deeper inside a wall.

find the largest-possible sensing distance (i.e., sensing range) for a given setting.

Figure 15 shows how the transmitter-receiver distance affects the sensing range of WIDESEE. We see that the sensing range in general grows as the transmitter-receiver distance increases. However, it reaches a plateau with a detectable distance of 53 m. This suggests that WIDESEE can achieve a sensing range of 53 m for a moving target in a relatively ideal environment (an open square). When the Tx-Rx distance exceeds 60 m, the sensing range drops rapidly. We believe this is because the human reflected signal becomes weaker and limits the contactless sensing range when the distance between the Tx and Rx is too far. While a 53 m sensing range is already a significant improvement over WiFi, RFID and mmWave-based systems, which have a sensing range below 6 m [54], [60], [66]. However, we believe there is a potential to further increase this sensing range with careful signal processing considering the kilometer-level communication range and we leave it as important future work.

2) Evaluation of Our Antenna System: This experiment is designed to evaluate the performance of our antenna system in human target detection. We compare our design against two alternative designs which use an omnidirectional [1] and a horn directional (RFMAX [5]) antenna with a similar size. Our testing area is an open square with a size of 42×48 m^2 depicted in Figure 14 (a). We divided the testing area into a grid of 224 blocks, 3×3 m^2 for each block. Like the previous experiment, we asked a human target to choose any block and then move within the block naturally. We ensure that each block was tested at least once.

Figure 16 shows that our design presents the best trade-off between the detection accuracy and area coverage. In this experiment, we report the number of detectable blocks. Note that this is different from the evaluation in Section IV-B.1, where we are interested in the longest-possible distance for detecting a target that is always on the perpendicular bisector of the transceiver pair. In this experiment, most of the blocks are not on the perpendicular bisector of the transceiver pair. As we increase the transmitter-receiver distance beyond 36 m, we see a decrease in the number of detectable blocks. This is mainly due to the directionality of the receiver antenna.

While RFMAX, the horn directional antenna achieves the second-best detection accuracy, it can detect the least number of blocks. The omnidirectional antenna, on the other hand, can cover more blocks, but it achieves the poorest detection accuracy due to its high sensitivity to the surrounding interference. The sensing range achieved by our antenna is relatively large due to the signal focusing and radiation direction switching, and it delivers a much higher detection accuracy for all settings. The better detection accuracy of our approach is largely attributed to its narrower beam, which in turn leads to a stronger signal and at the same time less interference from non-target objects.

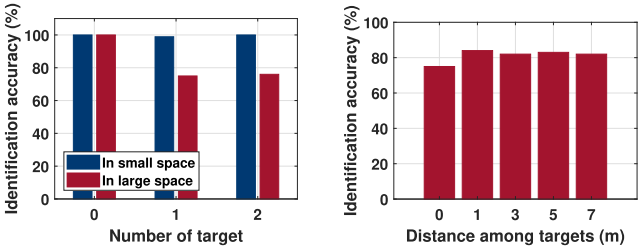

(a) Identification results in multi-target scenario.

(b) Impact of distance among targets.

Fig. 18. Multi-target detection accuracy.

3) Penetration Test: We also evaluate WIDESEE's ability to penetrate the walls. Experiments were conducted in the underground garage as shown in Figure 14 (b) and the second floor of our test building shown in Figure 14 (c). Our evaluation includes four settings – no wall and wall made of reinforced concrete with three different thicknesses (26 cm, 52 cm and 94 cm) between the target and the transceiver pair. In the through-wall experiment, we placed the transceiver pair 1.5 m away from the wall.

Figure 17 shows the results. As expected, the thinner the obstacle between the target and the transceiver pair, the deeper WIDESEE can successfully detect the target. We observe the target's activity also has a significant impact on the detectable distance. If the target is ambulating or waving, WIDESEE can successfully detect the target up to 15 m and 13 m, respectively. WIDESEE can also detect a stationary target with just respiration. However, the detection distance is limited and depends on the thickness of the wall. This is not surprising, as the smaller the activity and the thicker the wall is, the weaker the received signal strength will be. For our experiments, a 20 cm increase in the wall's thickness would reduce the received signal strength by around 29 dB. Nonetheless,

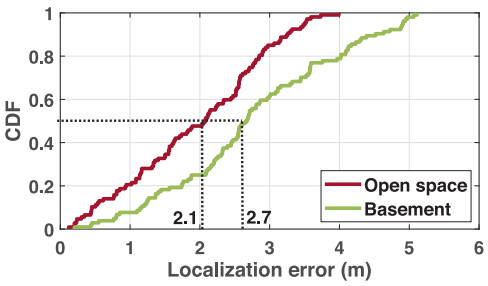

Fig. 19. CDF plots of the localization error in two large scenarios (10×25 m^2) with different densities of multipath.

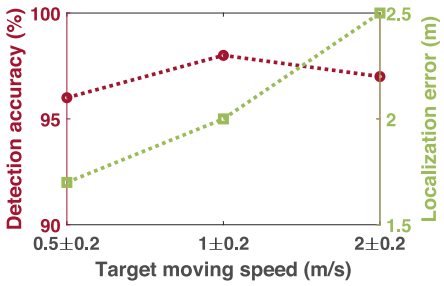

Fig. 20. Impact of target moving speed. The target's moving speed has little impact on detection, but it affects localization.

the results show that WIDESEE can accurately detect a human target moving or waving deep inside the building.

4) Multi-Target Detection Accuracy: We conducted multi-target detection experiment in both small space and large space scenarios. The small space scenario is in an indoor room with test area size of 3×6 m^2. The LoRa transceiver pair is placed 1 m away outside the room and separated by 3 m. The room wall is made of concrete cement and with a thickness of 50 cm. The large space scenario is in outdoor environment with test area size of 10×10 m^2, and the transceiver pair is separated by 10 m. In each scenario, we conducted experiments with different numbers of volunteer targets inside the room and the volunteers are allowed to walk randomly within the test area. For each target quantity, we continuously collected data for about 20 min and segmented the data at step size of 0.25 s. We used 2157 sets and 540 sets of data for SVM training and testing, respectively. The identification result is shown in Figure 18 (a), and we can see that WIDESEE achieves higher than 98% identification accuracy in small apace. The accuracy in large space decreases due to the weaker target reflection.

Impact of distance among targets. In this experiment, we investigated how the distance among targets affects the multi-target detection accuracy. The experiment was conducted in the large space scenario. We collected data of two targets separated by different distances and walking inside the test area. The data collected at each distance was used for training and testing in mul-target recognition model. Figure 18 (b) shows the identification accuracy of two targets at varying distances. We can see that when the distance is small as 0 m, the accuracy decreases. This is expected since there exists severe mutual occlusion when two targets are too close to each other.

5) Localization Accuracy in Different Multipath Environments: We report how multipath impacts localization accuracy in this section. Our evaluation environments are the open square (Figure 14 (a)) and basement parking garage (Figure 14 (b)). As can be seen in Figure 14 (b), the basement is supported by many pillars and hence has rich multipath. The test areas in both environments are of the same size (10×25 m^2), and we set the transmitter-receiver distance as 10 m. We divided the testing area into 125 blocks, where each block has a size of 2×1 m^2. For each block, a target was asked to walk following predefined straight lines that have $0°$, $30°$, $45°$, $60°$ or $90°$ degrees with respect to the transmitter-receive line. For each line, the user walked for around 2 s, starting from the center of a block. Figure 19 plots the cumulative distribution function (CDF) of the localization error across our 125 experiment trials. This diagram shows that for over 50% of our test cases, the localization error is within 2.1 m and 2.7 m in the open square and the basement, respectively. Such accuracy would be good enough for locating a human target in many application scenarios, demonstrating the great potential of sensing using a single LoRa transceiver pair.

We conduct another experiment to show the tracking accuracy of our system in a smaller area. This experiment was performed in a smaller room located in the building shown in Figure 14. The room has a size of 8×10 m^2. In this experiment, the transmitter-receiver distance is set as 6 m. The target was asked to walk along the trajectory of five letters "BCIMO". The recovered trajectories (dots) and the ground-truth trajectories (solid lines) are shown together in Figure 21. WIDESEE achieves a median localization error of 52 cm, which is comparable to the 32 cm error achieved in IndoTrack - a state-of-the-art WiFi tracking system with dense deployment [60]. This experiment shows that WIDESEE is able to track the target at higher accuracy in a smaller-size area.

6) Impact of the Target's Moving Speed: This experiment studies the effect of the target's walking speed on detection and localization. We consider three walking speeds: slow (0.5 ± 0.2 m/s), average (1 ± 0.2 m/s) and fast (2 ± 0.2 m/s). We conducted the experiments in the open square shown in Figure 14 (a).

Figure 20 shows that the target's moving speed has little impact on target detection, but it does affect the localization accuracy. We observe a localization error of 1.7 m, 2 m, and 2.5 m when the target was moving at slow, average, and fast speeds respectively. This is largely attributed to the body motions (e.g., arm swing) – the faster the walking speed is, the more drastic the body movement will be – a more drastic body movement makes it harder to satisfy the conditions that we use for localization (see Equation 7).

C. Building-Scale Field Study

In this field study, we employ WIDESEE with a drone (see also Figure 2) to perform building-scale sensing. The task is to detect and track a human target located on the 9^{th} floor of

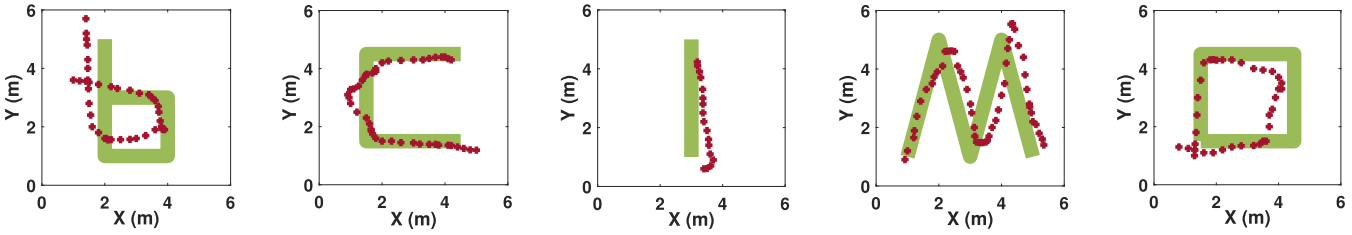

Fig. 21. Tracking results in a smaller room with size of $6 \times 8\ m^2$. The median tracking error of WIDESEE is $52\ cm$, which is comparable with a state-of-the-art that utilizes two WiFi transceiver pair [60].

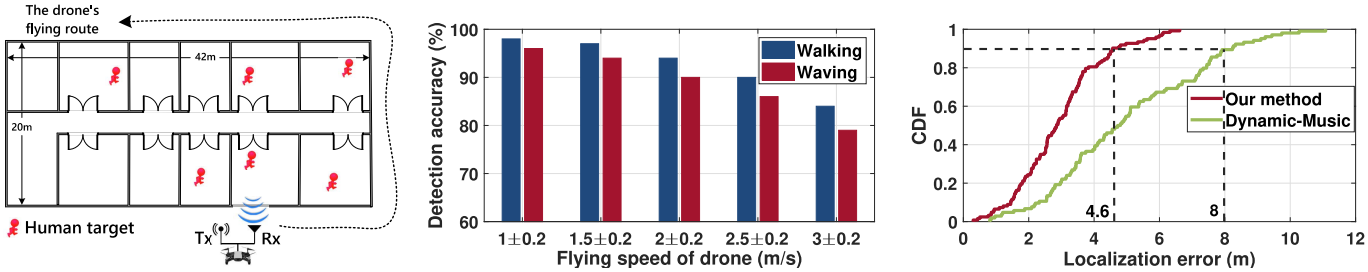

(a) Building-scale experimental setup.

(b) Target detection accuracy in building-scale field study, with various drone's flying speeds.

(c) CDF plots of the localization error given by our and Dynamic-Music's multipath elimination schemes.

Fig. 22. Building-scale experiments.

a 17-floor building structure with a size of $20 \times 42 \times 85\ m^3$ (Figure 14 (c)). Note that the drone needs to be static to the earth during the localization process based on our localization model, while it can be flying in the detection phase. Once we have detected a moving target, we hover the drone in place for two seconds to collect target-reflected signals, and apply the localization algorithms to estimate the target position. If no target is detected, the drone keeps flying. Also note that this new building had no occupant at the time of our experiment. The thicknesses of the concrete walls and glass windows are $40\ cm$ and $5\ cm$, respectively. The transceiver pair was carried by a drone in this experiment. The distance between the transmitter and the receiver is $2\ m$. Ten student volunteers participated in this study, serving as the target. Figure 22 (a) shows the experimental setup. The students were arranged into three groups to perform stationary (breathing) (2 students), waving (4 students) and walking (4 students) activities, and are located in rooms on the same floor. We manually controlled the drone to fly to an initial position of the 9^{th} floor, and used the software-based control module (Section III-B.2) to control the drone's fly. We varied the flying speed of the drone in the experiments.

1) Detecting Human Presences: Figure 22 (b) shows the detection accuracy for each human target who was walking and waving. When the drone was flying at a low speed of $1 \pm 0.2\ m/s$, WIDESEE can successfully detect 98% and 96% of the human targets who were walking and waving respectively. As expected, the detection accuracy decreases as the drone's speed increases, but WIDESEE is still able to detect the target most of the time when the target was walking or waving. WIDESEE is unable to detect the stationary (breathing) target in this study when the device is on a drone and the target is pretty far away ($> 5\ m$) from the device with a $40\ cm$ wall made of reinforced concrete in between. However, our current implementation would already be useful for disaster rescue to detect conscious survivors, many of whom tend to wave to attract the attention of rescuers.

2) Localization Accuracy: Figure 22 (c) compares the localization error of our approach with Dynamic-Music [61]. As we can see, our approach delivers a better localization accuracy over Dynamic-Music. It reduces the localization error from $8\ m$ to $4.6\ m$ for over 90% of the test cases. Although the $4.6\ m$ localization error is intuitively large, it allows us to identify which room or roughly which area of a building a human target is located. This is particularly useful in disaster rescue where we critically need to narrow down the search area for survivors. Note that although our localization algorithm is a 2D model, we can roughly determine the vertical information of target according to the radiation range of reconfigurable antenna, which is verified in our pre-experiment. When multiple people scattered at different floors but the same direction, we can locate each target in turn by flying drones across different floors.

V. DISCUSSIONS

As the first attempt in applying LoRa signals for sensing, there is room for improvement and further work. We discuss a few issues here.

Non-moving target localization. We are able to detect non-moving human target through sensing his/her respiration or in-place activities such as waving. Note that the sensing range of through-wall respiration sensing is still limited, since the signal attenuation caused by walls is significant and the signal variation induced by respiration movement (around $5\ mm$

chest displacement) is small and can easily be buried in noise. We plan to explore the feasibility of utilizing beamforming technology [26], [63], [70] to amplify the weak reflected signal to increase the respiration sensing range in the future. Careful signal processing with an antenna array is another promising direction to increase the sensing range as demonstrated in Farsense [67].

Target localization with device movements. In this paper, we can localize the target with a single pair of transceiver when the target is moving. Note that our system cannot localize the target when the LoRa device is also moving. This is because we remove the dynamic multipath interference based on the fact that dynamic multipath reflected twice is much weaker than direct target-reflected signal. If the transmitter/receiver is also moving, the original static path will also become dynamic path, which may be stronger than the direct target-reflected signal and then we cannot get rid of the effect of dynamic multipath in this case, resulting in large localization errors.

Multiple-target localization. In multiple-target scenario, we can identify the number of targets from the composition signal, but we cannot perform multi-target localization under the current restricted conditions. Localizing multiple target means we need to match multiple peaks from the PSD map to multiple targets. However, it is very challenging to pick multiple useful peaks under the severe interference of dynamic multipath with a single transmitter-receiver pair and a limited channel bandwidth. In our future work, we plan to employ an antenna array to focus the transmission power at one direction and also exploit the blind signal separation algorithm [18], [65] to spatially separate mixed signals for multi-target localization.

Despite these limitations, WIDESEE moves an important step toward enabling wide-area contactless sensing. We believe WIDESEE provides valuable reference for future research in this field.

VI. RELATED WORK

Our work is broadly related to the literature in two areas.

A. Human Activity Recognition

Computer-vision-based human activity sensing techniques have enabled mature applications. For instance, Kinect [8] and Leap Motion [3] can achieve fine-grained human gesture tracking. However, these systems are sensitive to lighting condition and the monitoring angle and cannot work when the target is blocked or behind a wall. Infrared camera [35], [52] is insensitive to light and can achieve long-range sensing. However, it still cannot penetrate obstacles like walls. Wearable sensor-based solutions overcome the above limitations [15], [22], [33] but still bring in inconvenience to users as they require instrumenting the users. It would be unrealistic to assume every target has a working wearable in emergencies.

Compared to vision or wearable-based solutions, wireless-signal-based human activity recognition systems can penetrate walls and do not require the user to carry or wear a device. Typically, the UWB radar achieves accurate through-wall sensing based on the large bandwidth (i.e., several GHz) and narrow beam [36], [37], but the cost of specialized equipment that supports wall penetration is expensive. Early work in this area use multiple Wi-Fi transceiver pairs to construct a 3D lattice of wireless links to identify the presence of human movements [50]. Later works try to use a single device equipped with multiple antennas to realize activity recognition. For example, WiSee can differentiate nine commonly seen body gestures with the help of machine learning techniques [48]. The effectiveness of the learning based methods depends on the quality of the training data. On the other hand, obtaining high quality training data remains costly and non-trivial. For example, CrossSense [25] requires collecting thousands of samples to learn a single activity recognition model at one given environment. WIDESEE avoids the pitfalls of a learning-based approach by developing analytical models for activity recognition. It requires significantly less effort for collecting data samples and can be portable to different environments.

Recent studies also show it is possible to sense the respiration [9], [17], [20], [64], [71], [72], heart rate [9], or even emotion [42] using wireless signals. However, prior approaches only work at a small scale (e.g., the room-level) and would require dense deployment to work on a large area. WIDESEE builds upon these past foundations of human activity modeling, to extend the scope of contactless human sensing for wide areas with a LoRa transceiver pair. Our work aims to close the gap of wireless sensing for disaster rescue in the urban areas, as well as terrorist search and security surveillance.

B. Indoor Localization and Tracking

There is an intensive body of work in localizing and tracking objects [11], [12], [24], [57], [60], [70]. Prior work can be broadly grouped into two categories: device-based and device-free approaches.

A device-free approach has the advantage of not requiring the end-user to carry a device. By lifting the limitation of carrying a device, device-free methods can target a wider range of applications when compared to the device-based counterparts. WIDESEE thus follows a device-free (contactless) approach.

Target localization and tracking can be realized through a range of wireless signal characteristics, including AoA [24], [34], ToF [10], [33], [40], and the signal attenuation [31]. An attenuation-based approach is simple and cost-efficient, but it suffers from poor localization accuracy (especially in non-line-of-sight conditions) – due to additional signal attenuation resulted from obstacles and severe amplitude fluctuation due to rich multipath indoors. Methods using phase information such as AoA-based localization can effectively separate multipaths, and a good resolution and accuracy would require a large antenna array at the receiver. ToF-based methods are not ideal either, because they are limited by the frequency bandwidth. More recent attempts leverage SAGE algorithm to jointly estimate multi-dimensional Wi-Fi link parameters for tracking [47], [65], while these systems still require multiple antennas at the receiver. In contrast, Learning based target localization algorithm [13], [58], [62] can overcome the multipath limitation of model based localization approaches, while it requires astronomic amount of training that comes at

high human cost. In addition, most of the existing technologies focus on room-scale tracking range due to the limited range of signal itself.

WIDESEE is the first attempt to realize contactless wide-area sensing with a single LoRa transceiver pair. It does so by combing the long-communication LoRa signal and the mobility of the drone. However, achieving the goal requires overcoming two challenges: (1) the serve multipath effects when using single LoRa transceiver pair, and (2) the hurdle for not having available phase or ToF information on LoRa. Inspired by [32], [46], WIDESEE extracts direction-related information from amplitude measurements for localization, but it advances prior work by relying on a single instead of multiple transceiver pairs. WIDESEE employs a set of new algorithms to remove the localization ambiguity caused by one transceiver pair. WIDESEE also leverages and refines existing multipath removal methods [61]. The result is a promising solution using a single transceiver pair for wide-area contactless sensing, which could potentially open up many new research opportunities.

VII. CONCLUSION

This paper has presented WIDESEE, a hardware-software system that can perform wide-area wireless sensing using just one transceiver pair. WIDESEE utilizes LoRa signals to achieve better through-wall penetration and larger sensing range. To further widen the sensing area, WIDESEE employs drones to carry the transceiver to improve the sensing coverage. The combination of single LoRa transceiver pair and device mobility, however, brings new challenges of severe interference and sensing ambiguities (e.g., localization). To address these challenges, we design a set of techniques at the hardware and software layers, which can be applied to many wireless sensing applications. We believe WIDESEE moves an important step towards wide-area wireless sensing, and is highly attractive in real-world emergency scenarios like disaster rescue and terrorist search.

REFERENCES

[1] (2017). *TX915-JK-11*. [Online]. Available: https://m.tb.cn/h.3CfHtz1?sm=3a9293/

[2] (2018). *Gnuradio*. [Online]. Available: https://www.gnuradio.org/

[3] (2015). *Leap Motion*. [Online]. Available: https://www.leapmotion.com/

[4] (2018). *LimeSDR Mini*. [Online]. Available: https://limemicro.com/products/boards/limesdr-mini/

[5] (2015). *RFMAX S9028PCR Antenna*. [Online]. Available: https://www.atlasrfidstore.com/rfmax-s9028pcrj-s8658prj-rhcp-indoor-rfid-antenna-fcc-etsi/

[6] Semtech. (2016). *SX1276 Transceiver*. [Online]. Available: http://www.semtech.com/wireless-RF/RF-transceivers/sx1276/

[7] *Spreading Wings S1000*. (2015). [Online]. Available: https://www.dji.com/cn/spreading-wings-s1000/

[8] (2015). *X-box Kinect*. [Online]. Available: http://www.xbox.com/

[9] F. Adib, M. Hongzi, E. Z. Kabelac, D. Katabi, and R. C. Miller, "Smart Homes that monitor breathing and heart rate," in *Proc. 33rd Annu. ACM Conf. Hum. Factors Comput. Syst.*, 2015, pp. 837–846.

[10] F. Adib, Z. Kabelac, D. Katabi, and C. R. Miller, "3D tracking via body radio reflections," in *Proc. 11th USENIX Symp. Networked Syst. Design Implement. (NSDI)*, 2014, pp. 317–329.

[11] F. Adib, Z. Kabelac, and D. Katabi, "Multi-person localization via RF body reflections," in *Proc. USENIX Symp. Networked Syst. Design Implement. (NSDI)*, 2015, pp. 279–292.

[12] D. Ashutosh, C. Ayon, S. Karthikeyan, and R. Sampath, "Strackio: Tracking first responders inside-out," in *Proc. USENIX Symp. Networked Syst. Design Implement. (NSDI)*, 2019, pp. 1–14.

[13] R. Ayyalasomayajula *et al.*, "Deep learning based wireless localization for indoor navigation," in *Proc. 26th Annu. Int. Conf. Mobile Comput. Netw.*, Apr. 2020, pp. 1–14.

[14] J. T. Bernhard, "Reconfigurable antennas," *Synth. Lect. Antennas*, vol. 2, no. 1, pp. 1–66, 2007.

[15] B. Chen, V. Yenamandra, and K. Srinivasan, "Tracking keystrokes using wireless signals," in *Proc. 13th Annu. Int. Conf. Mobile Syst., Appl., Services*, May 2015, pp. 31–44.

[16] G. Chuhan, L. Yilong, and Z. Xinyu, "LiveTag: Sensing human-object interaction through passive chipless WiFi tags," in *Proc. 15th USENIX Symp. Networked Syst. Design Implement. (NSDI)*, 2018, pp. 533–546.

[17] Z. Fusang *et al.*, "From Fresnel diffraction model to fine-grained human respiration sensing with commodity Wi-Fi devices," in *Proc. ACM UbiComp*, 2018, pp. 1–23.

[18] H. Hassanieh, O. Abari, M. Rodriguez, M. Abdelghany, D. Katabi, and P. Indyk, "Fast millimeter wave beam alignment," in *Proc. Conf. ACM Special Interest Group Data Commun.*, Aug. 2018, pp. 432–445.

[19] Z. Hansong and Z. Yi, "Sensing movement: Microsensors for body motion measurement," *Sensors*, vol. 11, no. 1, pp. 638–660, 2011.

[20] H. Wang *et al.*, "Human respiration detection with commodity WiFi devices: Do user location and body orientation matter?" in *Proc. ACM Int. Joint Conf. Pervasive Ubiquitous Comput.*, Sep. 2016, pp. 25–36.

[21] A. Hassanien and S. A. Vorobyov, "Phased-MIMO radar: A tradeoff between phased-array and MIMO radars," *IEEE Trans. Signal Process.*, vol. 58, no. 6, pp. 3137–3151, Jun. 2010.

[22] W. He, T. T. Lai, and R. R. Choudhury, "Mole: Motion leaks through smartwatch sensors," in *Proc. 21st Annu. Int. Conf. Mobile Comput. Netw.*, 2015, pp. 155–166.

[23] C. W. Jakes, *Microwave Mobile Communications*. Hoboken, NJ, USA: Wiley, 1994.

[24] X. Jie and K. Jamieson, "ArrayTrack: A fine-grained indoor location system," in *Proc. 10th USENIX Symp. Networked Syst. Design Implement. (NSDI)*, 2013, pp. 71–84.

[25] J. Zhang, Z. Tang, M. Li, D. Fang, P. Nurmi, and Z. Wang, "CrossSense: Towards cross-site and large-scale WiFi sensing," in *Proc. 24th Annu. Int. Conf. Mobile Comput. Netw.*, Oct. 2018, pp. 305–320.

[26] W. Jingxian, Z. Junbo, S. Rajarshi, J. Haojian, and K. Swarun, "Pushing the range limits of commercial passive RFIDs," in *Proc. 16th USENIX Symp. Networked Syst. Design Implement. (NSDI)*, 2019, pp. 301–316.

[27] J. Gjengset, J. Xiong, G. McPhillips, and K. Jamieson, "Phaser: Enabling phased array signal processing on commodity WiFi access points," in *Proc. 20th Annu. Int. Conf. Mobile Comput. Netw.*, Sep. 2014, pp. 153–164.

[28] J. Wang *et al.*, "LiFS: Low human-effort, device-free localization with fine-grained subcarrier information," in *Proc. 22nd Annu. Int. Conf. Mobile Comput. Netw.*, Oct. 2016, pp. 243–256.

[29] J. Wang, J. Xiong, X. Chen, H. Jiang, R. K. Balan, and D. Fang, "TagScan: Simultaneous target imaging and material identification with commodity RFID devices," in *Proc. 23rd Annu. Int. Conf. Mobile Comput. Netw.*, Oct. 2017, pp. 288–300.

[30] M. Jusoh, T. Aboufoul, T. Sabapathy, A. Alomainy, and M. R. Kamarudin, "Pattern-reconfigurable microstrip patch antenna with multidirectional beam for Wimax application," *IEEE Antennas Wireless Propag. Lett.*, vol. 13, pp. 860–863, 2014.

[31] K. Wu, J. Xiao, Y. Yi, M. Gao, and L. M. Ni, "FILA: Fine-grained indoor localization," in *Proc. IEEE INFOCOM*, Mar. 2012, pp. 2210–2218.

[32] C. R. Karanam, B. Korany, and Y. Mostofi, "Magnitude-based angle-of-arrival estimation, localization, and target tracking," in *Proc. 17th ACM/IEEE Int. Conf. Inf. Process. Sensor Netw. (IPSN)*, Apr. 2018, pp. 254–265.

[33] P. Kodeswaran, R. Kokku, M. Mallick, and S. Sen, "Demultiplexing activities of daily living in IoT enabled smarthomes," in *Proc. IEEE 35th Annu. IEEE Int. Conf. Comput. Commun. (INFOCOM)*, Apr. 2016, pp. 1–9.

[34] M. Kotaru, K. Joshi, D. Bharadia, and S. Katti, "SpotFi: Decimeter level localization using WiFi," in *Proc. ACM Conf. Special Interest Group Data Commun.*, Aug. 2015, pp. 269–282.

[35] S. Lee, D. Har, and D. Kum, "Drone-assisted disaster management: Finding victims via infrared camera and lidar sensor fusion," in *Proc. 3rd Asia–Pacific World Congr. Comput. Sci. Eng. (APWC CSE)*, Dec. 2016, pp. 84–89.

[36] J. Li, Z. Zeng, J. Sun, and F. Liu, "Through-wall detection of human being's movement by UWB radar," *IEEE Geosci. Remote Sens. Lett.*, vol. 9, no. 6, pp. 1079–1083, Jun. 2012.

[37] X. Liang, T. Lv, H. Zhang, Y. Gao, and G. Fang, "Through-wall human being detection using UWB impulse radar," *EURASIP J. Wireless Commun. Netw.*, vol. 2018, no. 1, pp. 1–17, Dec. 2018.

[38] L. Zhang, Q. Gao, X. Ma, J. Wang, T. Yang, and H. Wang, "DeFi: Robust training-free device-free wireless localization with WiFi," *IEEE Trans. Veh. Technol.*, vol. 67, no. 9, pp. 8822–8831, Sep. 2018.

[39] L. Shangguan and K. Jamieson, "The design and implementation of a mobile RFID tag sorting robot," in *Proc. 14th Annu. Int. Conf. Mobile Syst., Appl., Services*, Jun. 2016, pp. 31–42.

[40] A. T. Mariakakis, S. Sen, J. Lee, and K.-H. Kim, "SAIL: Single access point-based indoor localization," in *Proc. 12th Annu. Int. Conf. Mobile Syst., Appl., Services*, Jun. 2014, pp. 315–328.

[41] S. Minaeian, J. Liu, and Y. J. Son, "Vision-based target detection and localization via a team of cooperative UAV and UGVs," *IEEE Trans. Syst., Man, Cybern., Syst.*, vol. 46, no. 7, pp. 1005–1016, Jul. 2016.

[42] M. Zhao, F. Adib, and D. Katabi, "Emotion recognition using wireless signals," in *Proc. 22nd Annu. Int. Conf. Mobile Comput. Netw.*, Oct. 2016, pp. 95–108.

[43] R. Nandakumar, S. Gollakota, and N. Watson, "Contactless sleep apnea detection on smartphones," in *Proc. 13th Annu. Int. Conf. Mobile Syst., Appl., Services*, May 2015, pp. 45–57.

[44] R. Nandakumar, V. Iyer, and S. Gollakota, "3D localization for sub-centimeter sized devices," in *Proc. 16th ACM Conf. Embedded Networked Sensor Syst.*, Nov. 2018, pp. 108–119.

[45] A. M. Noll, *Principles of Modern Communications Technology*. Norwood, MA, USA: Artech House, 2001.

[46] K. Qian, C. Wu, Z. Yang, Y. Liu, and K. Jamieson, "Widar: Decimeter-level passive tracking via velocity monitoring with commodity Wi-Fi," in *Proc. 18th ACM Int. Symp. Mobile Ad Hoc Netw. Comput.*, Jul. 2017, pp. 1–10.

[47] K. Qian, C. Wu, Y. Zhang, G. Zhang, Z. Yang, and Y. Liu, "Widar2.0: Passive human tracking with a single Wi-Fi link," in *Proc. 6th Annu. Int. Conf. Mobile Syst., Appl., Services*, 2018, pp. 350–361.

[48] Q. Pu, S. Gupta, S. Gollakota, and S. Patel, "Whole-home gesture recognition using wireless signals," in *Proc. 19th Annu. Int. Conf. Mobile Comput. Netw.*, 2013, pp. 27–38.

[49] Y. Sangki, C. YiChao, Z. Huihuang, Q. Lili, and M. Wenguang, "Strata: Fine-grained acoustic-based device-free tracking," in *Proc. 15th Annu. Int. Conf. Mobile Syst., Appl., Services*, Jun. 2017, pp. 15–28.

[50] L. Sun, S. Sen, D. Koutsonikolas, and K.-H. Kim, "WiDraw: Enabling hands-free drawing in the air on commodity WiFi devices," in *Proc. 21st Annu. Int. Conf. Mobile Comput. Netw.*, Sep. 2015, pp. 77–89.

[51] V. Talla, M. Hessar, B. Kellogg, A. Najafi, J. R. Smith, and S. Gollakota, "Lora backscatter: Enabling the vision of ubiquitous connectivity," *Proc. ACM Interact., Mobile, Wearable Ubiquitous Technol.*, vol. 1, no. 3, pp. 1–24, 2017.

[52] T. F. Tan, S. S. Teoh, J. E. Fow, and K. S. Yen, "Embedded human detection system based on thermal and infrared sensors for anti-poaching application," in *Proc. IEEE Conf. Syst., Process Control (ICSPC)*, Dec. 2016, pp. 37–42.

[53] T. Liu, L. Wan, Z. Qin, C. Qian, and X. Zhou, "Passive acoustic localization based on COTS mobile devices," in *Proc. IEEE 24th Int. Conf. Parallel Distrib. Syst. (ICPADS)*, Dec. 2018, pp. 299–306.

[54] T. Wei and X. Zhang, "MTrack: High-precision passive tracking using millimeter wave radios," in *Proc. 21st Annu. Int. Conf. Mobile Comput. Netw.*, Sep. 2015, pp. 117–129.

[55] T. Tomic *et al.*, "Toward a fully autonomous UAV: Research platform for indoor and outdoor urban search and rescue," *IEEE Robot. Autom. Mag.*, vol. 19, no. 3, pp. 46–56, Sep. 2012.

[56] D. Vasisht, S. Kumar, and D. Katabi, "Decimeter-level localization with a single WiFi access point," in *Proc. 13th USENIX Symp. Networked Syst. Design Implement. (NSDI)*, 2016, pp. 165–178.

[57] J. Wang and D. Katabi, "Dude, where's my card?: RFID positioning that works with multipath and non-line of sight," in *Proc. ACM SIGCOMM Conf.*, Aug. 2013, pp. 51–62.

[58] X. Wang, X. Wang, and S. Mao, "Deep convolutional neural networks for indoor localization with CSI images," *IEEE Trans. Netw. Sci. Eng.*, vol. 7, no. 1, pp. 316–327, Jan. 2020.

[59] W. Wang, A. X. Liu, and K. Sun, "Device-free gesture tracking using acoustic signals," in *Proc. 22nd Annu. Int. Conf. Mobile Comput. Netw.*, Oct. 2016, pp. 82–94.

[60] X. Li *et al.*, "IndoTrack: Device-free indoor human tracking with commodity Wi-Fi," *Proc. ACM Interact., Mobile, Wearable Ubiquitous Technol.*, vol. 1, no. 3, pp. 1–22, Sep. 2017.

[61] L. Xiang, L. Shengjie, Z. Daqing, X. Jie, and M. Hong, "Dynamic-MUSIC: Accurate device-free indoor localization," in *Proc. ACM Int. Joint Conf. Pervasive Ubiquitous Comput.*, Sep. 2016, pp. 196–207.

[62] J. Xiao, K. Wu, Y. Yi, L. Wang, and L. M. Ni, "Pilot: Passive device-free indoor localization using channel state information," in *Proc. IEEE 33rd Int. Conf. Distrib. Comput. Syst.*, Jul. 2013, pp. 236–245.

[63] F. Xiaoran *et al.*, "Energy-ball: Wireless power transfer for batteryless Internet of Things through distributed beamforming," *Proc. ACM Interact., Mobile, Wearable Ubiquitous Technol.*, vol. 2, no. 2, pp. 1–22, 2018.

[64] B. Xie and J. Xiong, "Combating interference for long range Lora sensing," in *Proc. 18th Conf. Embedded Networked Sensor Syst.*, Nov. 2020, pp. 69–81.

[65] Y. Xie, J. Xiong, M. Li, and K. Jamieson, "MD-Track: Leveraging multi-dimensionality for passive indoor Wi-Fi tracking," in *Proc. 25th Annu. Int. Conf. Mobile Comput. Netw.*, Aug. 2019, pp. 1–16.

[66] Y. Zou, J. Xiao, J. Han, K. Wu, Y. Li, and L. M. Ni, "GRfid: A device-free RFID-based gesture recognition system," *IEEE Trans. Mobile Comput.*, vol. 16, no. 2, pp. 381–393, Feb. 2017.

[67] Z. Youwe, W. Dan, X. Jie, Y. Enze, G. Ruiyang, and Z. Daqing, "Farsense: Pushing the range limit of WiFi-based respiration sensing with csi ratio of two antennas," *Proc. ACM Interact., Mobile, Wearable Ubiquitous Technol.*, vol. 3, no. 3, pp. 1–26, 2019.

[68] Y. Ma, N. Selby, and F. Adib, "Drone relays for battery-free networks," in *Proc. Conf. ACM Special Interest Group Data Commun.*, Aug. 2017, pp. 335–347.

[69] Y. Ma, N. Selby, M. Singh, and F. Adib, "Fine-grained RFID localization via ultra-wideband emulation," in *Proc. SIGCOMM Posters Demos*, Aug. 2017, pp. 116–118.

[70] Y. Ma, Z. Luo, C. Steiger, G. Traverso, and F. Adib, "Enabling deep-tissue networking for miniature medical devices," in *Proc. Conf. ACM Special Interest Group Data Commun.*, Aug. 2018, pp. 417–431.

[71] F. Zhang *et al.*, "Exploring Lora for long-range through-wall sensing," *Proc. ACM Interact., Mobile, Wearable Ubiquitous Technol.*, vol. 4, no. 2, pp. 1–27, Jun. 2020.

[72] F. Zhang *et al.*, "Unlocking the beamforming potential of Lora for long-range multi-target respiration sensing," *Proc. ACM Interact., Mobile, Wearable Ubiquitous Technol.*, vol. 5, no. 2, pp. 1–25, Jun. 2021.

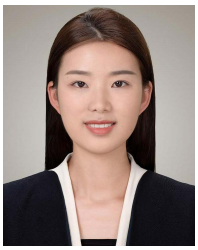

Lili Chen (Member, IEEE) received the Ph.D. degree from Northwest University. She is currently a Post-Doctoral Research Associate with Tsinghua University. Her current research interests include wireless systems and smart IoT. She is a member of ACM.

Kai Chen is currently pursuing the Ph.D. degree with the School of Information Science and Technology, Northwest University. His current research interests include wireless sensing and backscatter communication.

Jie Xiong (Member, IEEE) received the B.Eng. degree from University College London, the M.S. degree from Duke University, and the Ph.D. degree from Nanyang Technological University. He is currently an Assistant Professor with the College of Information and Computer Sciences, University of Massachusetts Amherst. His current research interests include wireless sensing, mobile health, smart IoT, and cyber-physical systems.

Ke Li (Member, IEEE) received the B.S. degree in electronic information engineering and the Ph.D. degree in electromagnetic wave and microwave technology from Xidian University, Xi'an, China, in 2011 and 2016, respectively. She is currently an Associate Professor with the School of Information Science and Technology, Northwest University, Xi'an. Her research interests include multiband antenna design, reconfigurable antennas, and metamaterials.

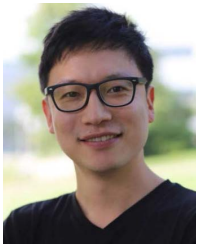

Sunghoon Ivan Lee (Senior Member, IEEE) received the Ph.D. degree in computer science from the University of California at Los Angeles in 2014. He is currently an Assistant Professor with the College of Information and Computer Sciences, University of Massachusetts Amherst. His main research interests include mobile and personalized health, wearable health sensing, embedded systems, sensor data analytics, and clinical science. He is a member of ACM.

Fuwei Wang received the Ph.D. degree from Xidian University, Xi'an, China, in 2014. He is currently an Associate Professor with the School of Information Technology, Northwest University, Xi'an. His research interests include antenna scattering, metamaterials, antenna array synthesis, and passive wireless sensing.

Zhanyong Tang (Member, IEEE) is currently a Professor with the School of Information Science and Technology, Northwest University. His current research interests include networks and systems security. He is a member of ACM.

Zheng Wang (Member, IEEE) is the Chair Professor of intelligent software technology with the School of Computing, University of Leeds; and a Turing Fellow with The Alan Turing Institute. His research focuses on programming languages, applied machine learning, and systems security. He is a member of ACM.

Dingyi Fang (Member, IEEE) received the Ph.D. degree in computer science from Northwestern Polytechnical University in 2001. He is a Professor with the School of Information Science and Technology, Northwest University. His current research interests include the Internet of Things, mobile and wireless computing, and information security. He is a member of ACM.

Xiaojiang Chen (Member, IEEE) received the Ph.D. degree in computer software and theory from Northwest University, Xi'an, China, in 2010. He is a Professor with the School of Information Science and Technology, Northwest University. His current research interests include RF-based sensing and performance issues in the Internet of Things. He is a member of ACM.